The metal-nonmetal transition of liquid phosphorus by *ab initio* molecular-dynamics simulations



2002 J. Phys.: Condens. Matter 14 3715

(http://iopscience.iop.org/0953-8984/14/14/304)

INSTITUTE OF PHYSICS PUBLISHING JOURNAL OF PHYSICS: CONDENSED MATTER

J. Phys.: Condens. Matter **14** (2002) 3715–3723 PII: S0953-8984(02)31942-8

# The metal–nonmetal transition of liquid phosphorus by *ab initio* molecular-dynamics simulations

**Yasuhiro Senda**[1], **Fuyuki Shimojo**[2] **and Kozo Hoshino**[2]

[1] Department of Computational Science, Faculty of Science, Kanazawa University, Kakuma-machi, Kanazawa, 920-1192, Japan
[2] Faculty of Integrated Arts and Sciences, Hiroshima University, Higashi-Hiroshima, 739-8521, Japan

Received 17 December 2001, in final form 20 February 2002
Published 28 March 2002
Online at stacks.iop.org/JPhysCM/14/3715

**Abstract**

We have carried out *ab initio* molecular-dynamics simulations for liquid phosphorus under high temperature and high pressure in order to investigate the microscopic mechanism of the recently observed liquid–liquid phase transition of liquid phosphorus. We have successfully shown by our simulation that the structural phase transition with increasing pressure corresponds to the structural change from the molecular liquid composed of stable tetrahedral $P_4$ molecules to the polymeric liquid with complex network structure and that the calculated structure factors are in good agreement with those obtained by the x-ray diffraction experiments. It is also found from our calculated electronic structure that this structural change gives rise to the nonmetal–metal transition, which is the transition from the nonmetallic molecular liquid to the metallic polymeric liquid.

## 1. Introduction

It is well known that phosphorus (P) shows a wide variety of structural forms at ambient pressure and temperature; a molecular solid, so-called 'white' P, comprising tetrahedral $P_4$ molecules, a variety of 'red' P, which are usually amorphous states, and an orthorhombic structure of 'black' P, consisting of puckered double layers of sixfold rings.

Recently, Katayama *et al* [1] have reported the x-ray diffraction results for a liquid–liquid structural phase transition in liquid P, involving an abrupt, pressure-induced structural change between two distinct liquid structures. They have shown that a small change of pressure at 1 GPa results in a reversible transformation and that the transformation is expected to be a first-order liquid–liquid phase transition from the low-density molecular liquid comprising tetrahedral $P_4$ molecules into the high-density polymeric liquid, accompanied by a discontinuous change in the density of liquid P.

As for the theoretical study on the structure of liquid P, Hohl and Jones [2] have performed *ab initio* molecular-dynamics (MD) simulations for the liquid phases of 'white' P and shown

  

that the $P_4$ tetrahedral molecules that exist in liquid P at room temperature break into a polymeric network at higher temperature under constant density. Their study showed that stable chemical bonds in the $P_4$ molecule break by thermally induced collisions between the $P_4$ molecules due to the high kinetic energy at high temperature. They only investigated the temperature effect on the structure of liquid P. Quite recently, Morishita [3] has applied constant-pressure *ab initio* MD simulation to liquid P and shown that the drastic change of the ionic configurations from the molecular liquid into the polymeric liquid is induced by the applied pressure during the simulations.

Although the electronic structures of the $P_4$ molecule have been investigated on the basis of the quantum chemistry [4,5], there have been few investigations for the electronic properties of liquid P under high pressure and high temperatures. Therefore, in this paper, we focus on the electronic properties, in particular, on the density or the pressure dependence of the electronic states of liquid P, which are closely related to the liquid–liquid structural phase transition.

In this paper we apply the *ab initio* MD simulations to the two liquid Ps, i.e. the low-density and the high-density liquids, corresponding to the low-pressure molecular liquid and the high-pressure polymeric liquid, respectively. The purposes of this study are (1) to investigate the structural and the electronic properties of both low-density and high-density liquids, (2) to provide the microscopic interpretation of the characteristic features of the observed structure factors and (3) to discuss the nonmetal–metal transition accompanying the structural phase transition.

## 2. Method

To study the structure and the electronic states of liquid P, we carry out an *ab initio* MD simulation, which is based on the density functional theory in the local-density approximation, the pseudopotential theory and the adiabatic approximation. We minimize the Kohn–Sham energy functional for a given ionic configuration by the conjugate-gradient method [6] and calculate the electron density and the forces acting on ions based on the Hellmann–Feynman theorem.

We use the norm-conserving pseudopotential proposed by Troullier and Martins [7] for the P atom. The non-local part of the pseudopotential is calculated using the Kleinman–Bylander separable form [8]. The exchange–correlation energy is calculated in the local-density approximation [9, 10]. The partial core correction [11] is taken into account to guarantee the transferability of the employed pseudopotential. The fractional occupancies of energy levels are introduced to ensure the convergence of the electronic states of metals. The wavefunction, only sampled at the $\Gamma$-point of the Brillouin zone, is expanded with the plane waves, and their cutoff energy is 15 Ryd, which is determined so as to converge the total energy to within 1 mRyd/electron.

In our calculations, a cubic supercell is used and the periodic boundary condition is imposed. The total number of atoms in the supercell is taken to be 100. The side of the cubic cell is about 13–17 Å. As an initial configuration, $P_4$ tetrahedral molecules are arranged on the simple-cubic lattice.

A constant-temperature MD simulation is carried out using the Nosé–Hoover thermostat technique [12, 13]. The classical equations of motion are solved using the velocity–Verlet algorithm. Our simulation is carried out for 7.2 ps with the time step of 3.6 fs after the thermal equilibrium state is achieved. The temperature is taken to be 1350 K and the observed densities [1] are used in our calculation for liquid P.

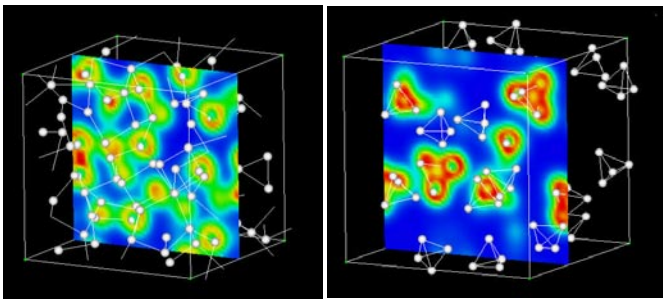

(a) (b)

**Figure 1.** The snapshots of ionic configurations and the electron density distribution for liquid P with (*a*) the high density $\rho = 2.8$ g cm$^{-3}$ and (*b*) the low density $\rho = 1.7$ g cm$^{-3}$. P ions are shown by white balls and the P–P bonds are drawn for P ion pairs within the cut-off distance of 2.6 Å.

## 3. Results and discussions

### *3.1. The structural properties*

In figures 1(*a*) and (*b*) we show the snapshots of the ionic configurations obtained by our *ab initio* MD simulations for the high-density liquid ($\rho = 2.8$ g cm$^{-3}$) and the low-density liquid ($\rho = 1.7$ g cm$^{-3}$), respectively, which show qualitatively different features. In the high-density liquid, the polymeric structure is obtained, where P–P bonds sometimes break and rearrange to form bonds with the other P ions. In the low-density liquid, the tetrahedral $P_4$ molecules are formed and they are very stable in the sense that they never break during our simulation. The existence of the strong chemical bonds within the $P_4$ molecules in the low-density liquid is evident from the electron density distribution with the bond charges as shown in figure 1(*b*) and also from the high first peak of the radial distribution function $g(r)$ as shown in figure 2. For the polymeric liquid the first peak of $g(r)$ is not so high and its structure has a similar feature to that of ordinary $s$–$p$ liquid metal. The position of the first peak of $g(r)$, $r = 2.28$ Å, is consistent with the P–P bond length within $P_4$ tetrahedral molecules in the white P crystal.

The coordination number around a P atom is three for the perfect tetrahedral $P_4$ molecule. Figure 3 shows the distribution function $P(n)$, which is defined as the probability that a P ion has $n$ neighbouring P ions within the first coordination shell, of radius 2.6 Å. It is seen from figure 3 that twofold- and fourfold-coordinated ions are not found in the low-density liquid, which arises from the fact that perfect tetrahedral $P_4$ molecules are formed in the low-density liquid. For the high-density liquid, though $P(n)$ has the maximum at the threefold coordination, there exist a considerable number of P atoms with twofold and fourfold coordinations, which results from the fact that bond breaking and bond rearrangements occur frequently in the polymeric liquid P. The ionic structure of the high-density liquid is expected to reflect that of the amorphous 'red' P and orthorhombic 'black' P. This is evident from the bond-angle distribution of the high-density liquid, which shows the maximum in the range from 90° to 110°, corresponding to the bond angle 103° of the 'red' P and 96° and 103° of the 'black' P [14].

To compare our results of calculations with the experimental ones obtained from the x-ray diffraction by Katayama *et al* [1], we calculate the structure factors $S(k)$ which are defined by

$$S(k) = \frac{1}{N}\left\langle \left| \sum_{\mu=1}^{N} \mathrm{e}^{-\mathrm{i}\boldsymbol{k}\cdot\boldsymbol{r}_\mu} \right|^2 \right\rangle, \tag{1}$$

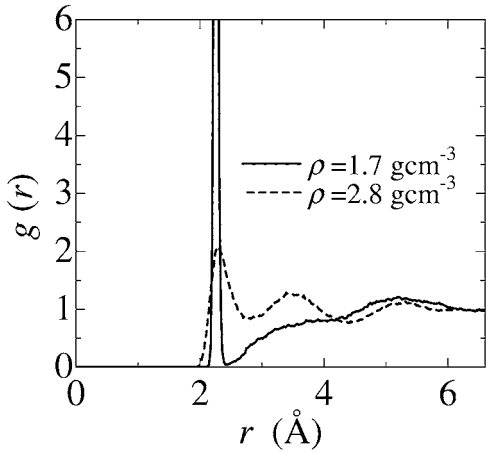


**Figure 2.** The $g(r)$ for liquid P with the low density (full curve) and the high density (broken curve).

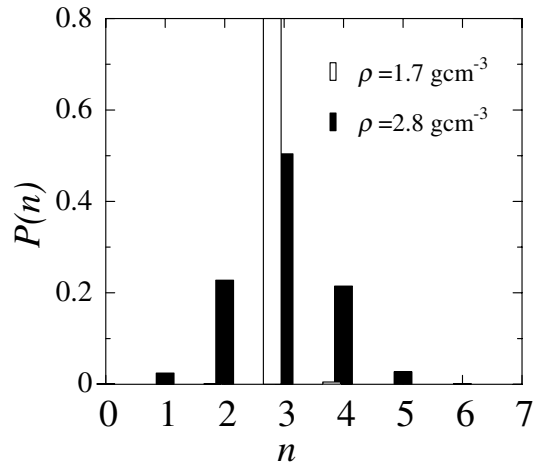


**Figure 3.** The distribution function $P(n)$ for the coordination number of P ions in liquid P.

using the positions of ions $\{\boldsymbol{r}_\mu\}$ obtained by our *ab initio* MD simulation. Here $N$ is the number of ions and the brackets $\langle\cdots\rangle$ mean the time average. Figure 4 shows the calculated structure factors and those obtained from x-ray diffraction. The calculated $S(k)$ for the high- and low-density liquid are in good agreement with the experimental results obtained for $P = 1.01$ GPa and $P = 0.77$ GPa, respectively. It should be noted from figure 4 that the characteristic feature of $S(k)$ changes drastically when the density or the pressure changes.

These features can be explained on the basis of the obtained ionic configurations. The high prepeak of $S(k)$ at $k \simeq 1.5$ Å$^{-1}$ in the low-density liquid originates from the correlation between $P_4$ tetrahedral molecules, which is evident from the correlation function $S_{tetra-tetra}(k)$ between the centre of mass of the tetrahedral $P_4$ molecules as shown in the upper panel of figure 4, where the main peak of $S_{tetra-tetra}(k)$ originates from the correlation between the $P_4$ tetrahedral molecules and its position corresponds to that of the prepeak of $S(k)$. It is therefore

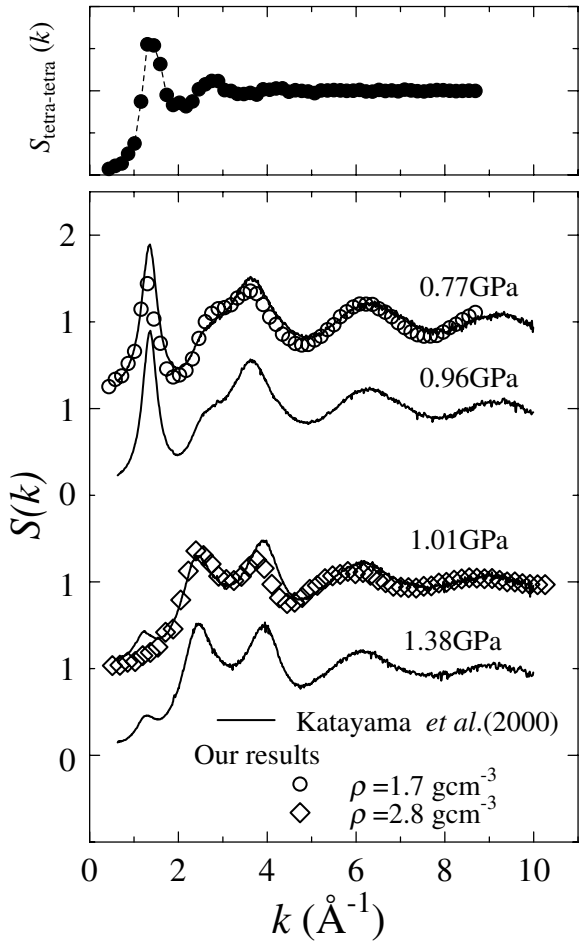


**Figure 4.** The bottom panel shows the $S(k)$ for liquid P with low density (open circles) and high density (open squares). The full curve shows the experimental results at the corresponding pressure. The upper panel shows the pair correlation function between the centres of mass of the $P_4$ tetrahedral molecules for the low-density liquid P.

concluded that the prepeak of $S(k)$ originates from the correlation between the $P_4$ tetrahedral molecules and also that the observed high prepeak proves the existence of stable $P_4$ tetrahedral molecules. The second peak of $S(k)$ originates from the mean distance of P atoms, since the value of $k \simeq 3.5$ Å$^{-1}$ corresponds, using the rule of thumb $kr = 7.7$ [15], to the reciprocal real-space distance $r \simeq 2.4$ Å at which the first peaks of $g(r)$ appear, as seen in figure 2.

We found the tendencies toward the first-order phase transition by performing the simulations at various densities ranging from the low density, $\rho = 1.7$ g cm$^{-3}$, to the high density, $\rho = 2.8$ g cm$^{-3}$. Beginning at $\rho = 1.7$ g cm$^{-3}$, we perform simulations with increasing density according to the above procedures of calculation. A sudden structural change from the molecular liquid to the polymeric liquid occurs at $\rho = 2.0$ g cm$^{-3}$, where there exist no stable $P_4$ tetrahedral molecules and the structural properties are similar to those of the polymeric liquid.

### *3.2. The electronic properties*

The electronic densities of states (DOSs) are obtained by sampling 10 $k$-points of the Brillouin zone and by averaging over some ionic configurations. The $l$th component of the DOS is calculated by projecting the wavefunctions on the spherical harmonics within a sphere of radius $R_c$ centred at each $\mu$th atom, the position of which is $\boldsymbol{r}_\mu$, as

$$D^l(\epsilon) = \sum_{\mu=1}^{N} \sum_{\alpha} \sum_{m=-l}^{l} \int_0^{R_c} |\boldsymbol{r} - \boldsymbol{r}_\mu|^2 \, \mathrm{d}|\boldsymbol{r} - \boldsymbol{r}_\mu| \left| \int Y_{lm}^*(\Omega_\mu) \psi_\alpha(\boldsymbol{r}) \, \mathrm{d}\Omega_\mu \right|^2 \delta(\epsilon - \epsilon_\alpha) \Big/ N, \quad (2)$$

where $N$ is the number of ions, $\psi_\alpha(\boldsymbol{r})$ is the wavefunction of the $\alpha$th state with the eigenvalue $\epsilon_\alpha$ and $Y_{lm}(\Omega_\mu)$ is the spherical harmonic with an angular momentum $l$, which is centred at the $\mu$th ion. $R_c$ is chosen to be about half of the average nearest-neighbour distance, on which the DOS does not depend significantly. Figures 5($a$) and ($b$) thus show the calculated total and partial DOSs for the high-density and the low-density liquid P, respectively, where the origin of the energy is taken to be the Fermi level.

We also show the distributions of the electron density in figures 1($a$) and ($b$), where the contour maps of the electron density distribution are displayed together with the ionic configurations.

*3.2.1. The metallic liquid.* It is seen from figure 5($a$) that the DOS below the Fermi level consists of two wide bands, and they spread around the atomic energy levels $3s$ and $3p$, which are indicated in the figure by solid circles. In the high-density liquid, the packing of P ions is dense, which leads to a large degree of overlap of $s$ and $p$ wavefunctions of the P atom, and gives rise to these wide energy bands. The band ranging from $-17$ to $-8$ eV is mainly contributed from the $s$ states and another band ranging from $-8$ eV to the Fermi level originates mainly from the $p$ states. A considerable amount of the states around the Fermi level, though a small dip exists there, indicates the metallic property of the high-density liquid P, which is also seen from the distribution of the electron density shown in figure 1($a$) as a spatially spreading distribution.

*3.2.2. The non-metallic liquid.* It is seen from figure 5($b$) that the DOS for the low-density liquid is quite different from that for the above-mentioned high-density liquid. The 's band' now splits into two narrow bands at around $-15$ and $-9$ eV, and also the 'p band' is divided into two bands, the Fermi level falling between these two bands. This electronic structure can be explained by association with that of the tetrahedral $P_4$ molecule, whose energy levels are indicated by solid triangles together with the degeneracies in the parentheses in figure 5($b$). It is seen from figure 5($b$) that the energies of the narrow bands correspond to the energy levels of the $P_4$ molecule. A small overlap of the molecular orbitals of the $P_4$ molecules leads to the narrow band widths for the low-density liquid P.

The feature of this band structure is characterized by the energy gap around the Fermi level, which is closely associated with the stable chemical bond within the $P_4$ tetrahedral molecule. We pick up two eigenstates from the calculated electronic states as indicated by arrows in figure 5($b$); one state is the highest occupied state (HOS) and the other is the lowest unoccupied state (LUS), and the distributions of wavefunctions of the two states are shown in figures 6($a$) and ($b$), respectively, together with the ionic configuration. The blue and red regions show the different signs of the wavefunction. The wavefunction of the HOS shows the same sign along the two P atoms within a $P_4$ tetrahedral molecule, which means that the HOS and the states with similar eigenenergies to it contribute to the bonding between two P atoms within the $P_4$ tetrahedral molecule. The wavefunction of the LUS, in contrast to that

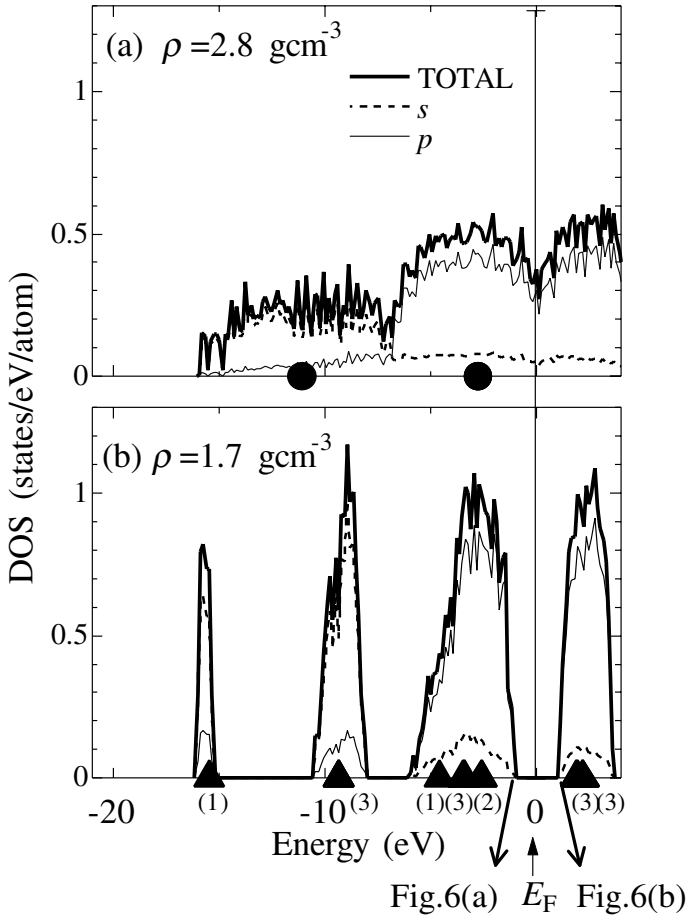


**Figure 5.** The total and the angular-momentum-decomposed density of states for (*a*) the high-density and (*b*) the low-density liquid P. The energy levels of a P atom and a tetrahedral $P_4$ molecule in the gas phase are indicated by the solid circles and the solid triangles, respectively, together with the degeneracies in parentheses.

of the HOS, shows the opposite sign between the two atoms, which indicates an anti-bonding character between the two P atoms, and so the LUS has an energy eigenvalue higher than that of the HOS. The Fermi level falls between the HOS and the LUS, which results in the non-metallic behaviour of the low-density liquid P.

This non-metallic property is also seen from the electron density distribution shown in figure 1(*b*). The electron density distribution is spatially localized around the $P_4$ tetrahedral molecules, in which the stable chemical bond is formed. This is in contrast to that of the metallic state of the high-density liquid P shown in figure 1(*a*).

### *3.3. Comparison of liquid P with the liquid alkali–Pb alloys*

We have found that liquid P shows a similar structural change as that of liquid alkali (Li, Na, K)–Pb alloys; there are tetrahedral $Pb_4$ molecules, which have similar properties as $P_4$ tetrahedral molecules have not only in their geometrical tetrahedral structure, but also in

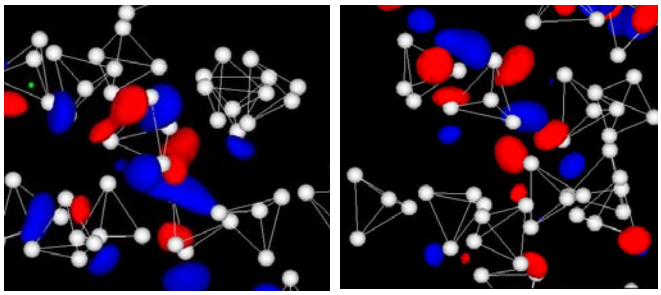

(a) (b)

**Figure 6.** The distributions of the wavefunction of (*a*) the highest occupied state and (*b*) the lowest unoccupied state, which are indicated by arrows in figure 5. The blue and the red regions show the opposite sign of the wavefunction.

the electronic structure [16–18]. We have carried out the *ab initio* MD simulations for some compositions of the liquid Li–Pb, Na–Pb and K–Pb alloys, and found that the polymeric structure of Pb ions is seen in the higher density of Pb ions, while the tetrahedral $Pb_4$ molecules exist stably when the number density of Pb atoms is lower. This is analogous to the structural transition of liquid P between the polymeric liquid and the molecular liquid composed of tetrahedral $P_4$ molecules. Moreover, it has been considered that the negatively charged $Pb_4^{4-}$ Zintl ions in the liquid alloys have the same electronic structure as the $P_4$ molecules [15, 17].

The DOS of the low- and the high-density liquid P have similar features to those of liquid alkali–Pb alloys. In the case of the liquid K–Pb alloys [17], the Pb-rich liquid alloys have wide bands of the partial DOS for Pb atoms. When the density of Pb ions is lower, the tetrahedral $Pb_4$ molecules are formed, and the electronic structure of the partial DOS for Pb changes into an assembly of narrow bands, which are related to the eigenenergies of the $Pb_4$ molecule.

## 4. Conclusion

The structural and the electronic properties of liquid P under high temperature and high pressure are investigated by *ab initio* MD simulations in order to clarify the microscopic mechanism of the observed liquid–liquid structural phase transition of liquid phosphorus. For the low-density liquid, tetrahedral $P_4$ molecules exist as isolated molecules with high stability and they do not break within our simulation time. For the high-density liquid, on the other hand, no tetrahedral structure is found, but rather a complex polymeric structure of liquid P is seen. From these structural properties and the electronic properties obtained by our *ab initio* MD simulations, we can conclude that the liquid–liquid phase transition observed by Katayama *et al* in liquid P corresponds to the structural change from the molecular liquid to the polymeric liquid.

It is also found from the electronic structure obtained by our simulation that this structural transition is accompanied by the metal–nonmetal transition between these two phases and that the mechanics of the metal–nonmetal transitions is closely associated with the existence of the $P_4$ molecules. We have explained the microscopic mechanism of the metal–nonmetal transition on the basis of the calculated electronic states and the ionic configurations.

## Acknowledgments

We are grateful to Dr Y Katayama for providing us with experimental data. This research is supported by Research and Development Applying Advanced Computational Science and Technology of the Japan Science and Technology Corporation (ACT-JST) and a Grant-in-Aid for Scientific Research from the Ministry of Education, Science, Sports and Culture, Japan. Calculations were performed using the Fujitsu VPP700E supercomputer of the Division of Computers and Information of the Institute of Physical and Chemical Research (RIKEN) and the Fujitsu VPP5000 supercomputer of the Computer Centre of Kyushu University.

## References

[1] Katayama Y, Mizutani T, Utsumi W, Shimomura O, Yamakata M and Funakoshi K 2000 *Nature* **403** 6766
[2] Hohl D and Jones R O 1994 *Phys. Rev.* B **50** 17 047
[3] Morishita T 2001 *Phys. Rev. Lett.* **87** 105701
[4] Hart R R, Robin M B and Kuebler N A 1965 *J. Chem. Phys.* **42** 3631
[5] Goodman N B, Ley L and Bullett B W 1983 *Phys. Rev.* B **27** 7440
[6] Shimojo F, Zempo Y, Hoshino K and Watabe M 1995 *Phys. Rev.* B **52** 9320
[7] Troullier N and Martins J L 1991 *Phys. Rev.* B **43** 1993
[8] Kleinman L and Bylander D M 1982 *Phys. Rev. Lett.* **48** 1425
[9] Ceperley D M and Alder B J 1980 *Phys. Rev. Lett.* **45** 566
[10] Perdew J P and Zunger A 1981 *Phys. Rev.* B **23** 5048
[11] Louie S G, Froyen S and Cohen M L 1982 *Phys. Rev.* B **26** 1738
[12] Nosé S 1984 *Mol. Phys.* **52** 255
[13] Hoover W G 1985 *Phys. Rev.* A **31** 1695
[14] Donohne J 1974 *The Structure of the Elements* (New York: Wiley) ch 8
[15] van der Lugt W 1996 *J. Phys.: Condens. Matter* **8** 6115
[16] Senda Y, Shimojo F and Hoshino K 1999 *J. Phys.: Condens. Matter* **11** 2199
[17] Senda Y, Shimojo F and Hoshino K 1999 *J. Phys.: Condens. Matter* **11** 5387
[18] Senda Y, Shimojo F and Hoshino K 2000 *J. Phys.: Condens. Matter* **12** 6106